



**HAL**  
open science

## Essential role of the CD docking motif of MPK4 in plant immunity, growth, and development

Anna Siodmak, Umar F Shahul Hameed, Naganand Rayapuram, Ronny Völz, Marie Boudsocq, Siba Alharbi, Hannah Alhoraibi, Yong-hwan Lee, Ikram Blilou, Stefan T Arold, et al.

### ► To cite this version:

Anna Siodmak, Umar F Shahul Hameed, Naganand Rayapuram, Ronny Völz, Marie Boudsocq, et al.. Essential role of the CD docking motif of MPK4 in plant immunity, growth, and development. *New Phytologist*, In press, 10.1111/nph.18989 . hal-04109431

**HAL Id: hal-04109431**










**<https://hal.science/hal-04109431>**

Submitted on 30 May 2023

**HAL** is a multi-disciplinary open access archive for the deposit and dissemination of scientific research documents, whether they are published or not. The documents may come from teaching and research institutions in France or abroad, or from public or private research centers.

L'archive ouverte pluridisciplinaire **HAL**, est destinée au dépôt et à la diffusion de documents scientifiques de niveau recherche, publiés ou non, émanant des établissements d'enseignement et de recherche français ou étrangers, des laboratoires publics ou privés.

# Essential role of the CD docking motif of MPK4 in plant immunity, growth, and development

Anna Siodmak<sup>1\*</sup> , Umar F. Shahul Hameed<sup>2\*</sup> , Naganand Rayapuram<sup>1</sup> , Ronny Völz<sup>3</sup> , Marie Boudsoq<sup>4</sup> , Siba Alharbi<sup>2</sup>, Hannah Alhoraibi<sup>5</sup>, Yong-Hwan Lee<sup>3,6,7,8</sup> , Ikram Blilou<sup>1</sup> , Stefan T. Arold<sup>2,9</sup>  and Heribert Hirt<sup>1,10</sup> 

<sup>1</sup>Plant Science Program, Center for Desert Agriculture, King Abdullah University of Science and Technology, Thuwal 23955-6900, Saudi Arabia; <sup>2</sup>Bioscience Program, Computational Bioscience Research Center (CBRC), King Abdullah University of Science and Technology (KAUST), Thuwal 23955-6900, Saudi Arabia; <sup>3</sup>Research Institute of Agriculture and Life Sciences, Seoul National University, Seoul 08826, Korea; <sup>4</sup>Université Paris Saclay, CNRS, INRAE, Univ Evry, Université Paris Cité, Institute of Plant Sciences Paris-Saclay IPS2, 91190 Gif sur-Yvette, France; <sup>5</sup>Department of Biochemistry, Faculty of Science, King Abdulaziz University, Jeddah 21551, Saudi Arabia; <sup>6</sup>Center for Fungal Genetic Resources, Seoul National University, Seoul 08826, Korea; <sup>7</sup>Department of Agricultural Biotechnology, Seoul National University, Seoul 08826, Korea; <sup>8</sup>Plant Immunity Research Center, Seoul National University, Seoul 08826, Korea; <sup>9</sup>Centre de Biologie Structurale (CBS), INSERM, CNRS, Université de Montpellier, F-34090 Montpellier, France; <sup>10</sup>Max Perutz Laboratories, University of Vienna, Dr. Bohrgasse 9, 1030 Vienna, Austria

## Summary

- MAPKs are universal eukaryotic signaling factors whose functioning is assumed to depend on the recognition of a common docking motif (CD) by its activators, substrates, and inactivators.
- We studied the role of the CD domain of Arabidopsis MPK4 by performing interaction studies and determining the ligand-bound MPK4 crystal structure.
- We revealed that the CD domain of MPK4 is essential for interaction and activation by its upstream MAPKKs MKK1, MKK2, and MKK6. Cys181 in the CD site of MPK4 was shown to become sulfenylated in response to reactive oxygen species *in vitro*. To test the function of C181 *in vivo*, we generated wild-type (WT) MPK4-C181, nonsulfenylatable MPK4-C181S, and potentially sulfenylation mimicking MPK4-C181D lines in the *mpk4* knockout background. We analyzed the phenotypes in growth, development, and stress responses, revealing that MPK4-C181S has WT activity and complements the *mpk4* phenotype. By contrast, MPK4-C181D cannot be activated by upstream MAPKK and cannot complement the phenotypes of *mpk4*.
- Our findings show that the CD motif is essential and is required for activation by upstream MAPKK for MPK4 function. Furthermore, growth, development, or immunity functions require upstream activation of the MPK4 protein kinase.

Authors for correspondence:

Stefan T. Arold

Email: [stefan.arold@kaust.edu.sa](mailto:stefan.arold@kaust.edu.sa)

Heribert Hirt

Email: [heribert.hirt@kaust.edu.sa](mailto:heribert.hirt@kaust.edu.sa)

Received: 7 April 2022

Accepted: 28 March 2023

New Phytologist (2023)

doi: 10.1111/nph.18989

**Key words:** immunity, kinase activity, MPK4, oxidation, reactive oxygen species.

## Introduction

Mitogen-activated protein kinases (MAPKs) constitute one of the most studied eukaryotic signaling mechanisms, comprising a class of proteins that play an essential role in linking perception of stimuli with several cellular and adaptive responses. The MAPK signal transduction pathways are minimally composed of distinct combinations of at least three protein kinases: a MAPKKK, a MAPKK, and a MAPK, which activate each other in a sequential manner via phosphorylation (Colcombet & Hirt, 2008). An activated MAPKKK first phosphorylates two serine and/or threonine residues (S/T-X3 – 5-S/T) located within the activation loop of the MAPKK. Activated MAPKKs in turn trigger MAPK activation through dual phosphorylation of a highly conserved T-X-Y

motif in the activation loop. The sequential activation of the MAPK cascade results in the phosphorylation of specific targets in response to specific extracellular stimuli (Bigeard *et al.*, 2015).

As for all kinases, the activity of MAPKs must be under tight spatiotemporal control. MAPKs phosphorylate substrates with the consensus sequence Ser/Thr-Pro. This simple pattern alone, however, is insufficient to assure the specific recognition of upstream activators and downstream substrates and inactivators. Based on structural and functional studies in animals and yeast, most MAPKs have a CD domain in their C-terminal region, which is a docking site for MAPKKs, MAPK phosphatases, and substrates and corresponds to the amino acid sequence [LH][LHY]Dxx[DE]xx[DE]EPxC (Tanoue *et al.*, 2000). On the contrary, most MAPK ligands, such as MAPKKs, MAPK phosphatases, and substrates have a putative MAPK docking site (D-site), which corresponds to the amino acid sequence [K/R][K/R][K/R]

\*These authors contributed equally to this work.

$x(1-5)[L/I]x[L/I]$  and which binds the MAPK CD domain (Bardwell, 2006). However, the existence of the CD domain–D-site recognition and its importance for MAPK signaling has not yet been experimentally established in plants.

Among *Arabidopsis* MAPKs, MPK4 is expressed in all plant tissues and functions in cytokinesis (Kosetsu *et al.*, 2010; Suzuki *et al.*, 2016), reproduction (Zeng *et al.*, 2011; Völz *et al.*, 2022), and growth (Gawroński *et al.*, 2014). In addition, MPK4 regulates the response to diverse stresses, such as cold (Du *et al.*, 2017), oxidative stress (Takáč *et al.*, 2016), or pathogens (Petersen *et al.*, 2000). Among biotic challenges, bacteria induce a plant immune mechanism called pattern-triggered immunity (PTI) which is controlled by several kinase cascades. MPK4 is part of several kinase cascades, composed of MEKK1-MKK1/2/6-MPK4 (Ichimura *et al.*, 2006; Nakagami *et al.*, 2006; Suarez-Rodriguez *et al.*, 2007; Lian *et al.*, 2018). Whereas MEKK1-MKK2 and MEKK1-MKK1 mediate salt and drought as well as H<sub>2</sub>O<sub>2</sub>-induced MPK4 activation, respectively (Teige *et al.*, 2004), MKK6 serves to regulate MPK4 in the context of cytokinesis (Kosetsu *et al.*, 2010) and PAMP signaling (Lian *et al.*, 2018). MPK4 is a negative regulator of plant immunity (Petersen *et al.*, 2000) that is activated by phosphorylation through its upstream signaling components MKK1/MKK2/MKK6 (Gao *et al.*, 2008; Lian *et al.*, 2018), thereby coordinating basal resistance and effector-triggered immunity (ETI; Zhang *et al.*, 2012). The effect of MPK4 is counter-balanced by the opposing actions of the MAPKs MPK3 and MPK6 (Bigeard *et al.*, 2015). The integrity of the MPK4 cascade is guarded by the R protein nucleotide-binding leucine-rich repeat (NB-LRR) protein SUPPRESSOR OF *mkk1 mkk2* (SUMM2) and SNM1 (Zhang *et al.*, 2016; Takagi *et al.*, 2019). SUMM2 monitors the phosphorylation of MPK4 substrates such as CALMODULIN-BINDING RECEPTOR LIKE KINASE 3 (CRCK3/SUMM3; Zhang *et al.*, 2016). CRCK3 associates with SUMM2 *in planta* and might act as a decoy or guard of SUMM2. Inactivation of MPK4 by pathogenic effectors, for example, HopA11 of *Pseudomonas*, reduces CRCK3 phosphorylation, and eventually activates SUMM2 to trigger autoimmunity and PCD (Zhang *et al.*, 2016), as seen for MPK4-deficient mutant plants. MPK4 downstream targets include transcription factors, which influence pathogenesis-related (*PR*) gene expression and the homeostasis of reactive oxygen species (ROS; Pitzschke *et al.*, 2009).

Recent investigations identified *Arabidopsis* MPK4 as oxidation target in a hydrogen peroxide dependent sulfenome screen of *Arabidopsis* cell cultures. Additional *in vitro* experiments revealed thiol oxidation of MPK4 on cysteine residues at positions C181 and C341 into sulfenic acid (Huang *et al.*, 2019). *Arabidopsis* MPK4 is the homolog of the human extracellular signal-related kinase2 (ERK2) also known as HsMAPK1. Amino acid sequence comparisons of MPK4 with ERK2 indicated that MPK4-C181 is conserved in human ERK2, corresponding to ERK2-C161. This region differentiates mitogen-activated protein (MAP) kinases from other kinases and is part of the MAPK docking motif that is important for interaction of MAPKs with their activating MAPK kinases and downstream substrates making this site particularly interesting for investigation (Dorin

*et al.*, 1999). For MPK4 and ERK2, the cysteines display the same structural environment, with a conserved histidine positioned close to the Cys (MPK4-His145 and ERK2-His125). This histidine might function as hydrogen ion acceptor, thereby decreasing the pK<sub>a</sub> of the cysteine and making it more susceptible to oxidation (Huang *et al.*, 2019). Investigations of human ERK2 showed that S-sulfenylation reduces ERK2 kinase activity (Keyes *et al.*, 2017). Moreover, Huang *et al.* (2019) showed that serine substitution of C181 (MPK4-C181S) resulted in strong reduction of MPK4 kinase activity *in vitro*, suggesting that C181 might play an important role in regulating the MPK4 pathway. We therefore investigated the molecular and organismal role of the docking domain and C181 on the functioning of MPK4 in growth, development, pathogen resistance, and oxidative stress. By structural analysis, we found that C181 is located in a position in the MPK4 CD domain critical for binding the D-site motif of MAPKs. Our genetic analysis shows that C181S does not affect kinase activity, plant development, or stress resistance but that C181D inhibits binding to activators of MPK4, resulting in a compromised kinase that is unable to be activated by its upstream activating MAPKs.

## Materials and Methods

### Plant material and culture conditions

For generation of complementation and mutant lines, which were generated in *Arabidopsis* ecotype Col-0, *mpk4-2* (SALK\_056245; Kosetsu *et al.*, 2010) was grown in soil under long-day conditions in the growth room. Six-week-old heterozygous plants were stably transformed and selected for three generations to obtain homozygous stable lines. Three different lines were prepared for each mutant and complementation, except C181D with two independent lines. For fresh weight and dry weight measurement, plants were grown on ½-strength Murashige & Skoog medium (½MS) and analyzed on Day 21. For root length measurement, plants were grown on ½MS medium and analyzed on Day 16.

### Seedling treatment

Seeds were sterilized, stratified at 4°C for 3 d, and grown vertically on ½MS solid medium (MS5524; Sigma) containing 0.5 g l<sup>-1</sup> MES, pH 5.7 and 1% (w/v) agar (A1296; Sigma), in a controlled chamber (22°C, 70% relative humidity, 16 h photoperiod at 100 μmol m<sup>-2</sup> s<sup>-1</sup>) for 14 d. This allowed us to select *mpk4*<sup>-/-</sup> seedlings based on the root phenotype (i.e. shorten, thicken, and agravitropic primary root; Kosetsu *et al.*, 2010) among *mpk4* and *mpk4:MPK4-PC2-C181D* lines, in which the *mpk4-2* mutation was segregating. For kinase assays, selected seedlings were transferred to liquid ½MS medium for overnight equilibration before applying mock (H<sub>2</sub>O) or 1 μM flg22 for 15 min. To stop treatment, seedlings were quickly dried, frozen in liquid nitrogen, and stored at -80°C. Each experiment was performed for all lines with three biological repeats. *Arabidopsis thaliana* ecotype Columbia-0 (Col-0) was used as wild-type

(WT) plant. For the rest of the experiments, plants were grown, treated, and harvested as described in Rayapuram *et al.* (2014).

### Gene synthesis and cloning

Primers for MPK4 mutant generation were designed according to the formula:  $69.3 + 0.41 \times A - 650/B$  ( $A$  = GC ratio of the primer,  $B$  primer length). It was aimed to reach an annealing temperature of 58–60°C and a length of 23–28 base pairs. The *mpk4-2* in Columbia-0 background (SALK\_056245) harbors a T-DNA insert in the sixth exon of the *MPK4* gene. The position of insertion was genotyped with a pair of gene-specific primers, INSMPK4 and RP, and with LBa1, and T-DNA insertion-specific primer (Supporting Information Table S1). The extraction of gDNA from plant leaves of *mpk4-2* mutants was performed as described by Edwards *et al.* (1991). The PCR on the isolated gDNA was carried out using Dream Taq DNA Polymerase according to the manufacturer's instructions, and the PCR cycling conditions are as described in Table S2. The genotyping was performed, including the use of a negative and positive control. The PCR products were electrophoresed and analyzed on a 2% Agarose gel. MPK4 gene was amplified and mutated performing a two-step PCR. Successfully amplified products were separated on an agarose gel and extracted by the QIAquick Gel Extraction Kit (28706; Qiagen, Germantown, MD, USA). Amplified gene products were sequenced by Sanger Sequencing Service, and the results were analyzed with CLC GENOMICS workbench software. The purified gene amplicons were restriction digested with PstI and XhoI and ligated into pGreen229-PC2 vector for protein expression.

Plasmid DNA purification was performed using QIAprep Spin Miniprep Kit as per the manufacturer's instruction. Vectors with the different genes of interest were amplified in *Escherichia coli* DH5 $\alpha$  cells. Transformed *E. coli* cells were cultivated at 37°C on LB plates or liquid LB media containing Kanamycin (50  $\mu\text{g ml}^{-1}$ ).

### Transgenic lines

Complementation and mutant lines were generated using pGreen229-PC2 vector driven by the MPK4 native promoter in *Arabidopsis mpk4-2* mutant background. The complementation of *mpk4-2* mutants was achieved inserting MPK4 WT, or MPK4 with mutations at C181S/D. Stable transformation was performed using *Agrobacterium tumefaciens* C58C1 of flowering *Arabidopsis* plants using the floral dip method. Positively transformed plants were isolated by spraying with BASTA solution (100  $\text{mg l}^{-1}$ ) twice at Days 8 and 13. For determination of transformation rates, T3 seeds were grown on  $\frac{1}{2}$ MS media with BASTA (10  $\text{mg l}^{-1}$ ). The transformation ratio was determined by counting the amount of nonresistant plants in comparison with all plants.

### Differential-contrast observation of *Arabidopsis* ovules

The oldest closed flower bud was emasculated. After 48 h, the entire flower was cleared in Corney's solution (9:1 ratio of

100% ethanol and acetic acid) for 24 h. Subsequently, the samples were rehydrated by using 80% and 70% ethanol for a half-hour each. The pistil was separated from the flower and mounted on an object slide in 40  $\mu\text{l}$  visikol (optical clearing agent). Afterward, the pistil was opened by the use of fine needles to release the ovules and covered by a cover slide followed by microscopical differential-contrast observation.

### Subcellular localization

Coding sequences of candidate genes were cloned in fusion with GFP at their C- and N-terminal parts under the control of the CaMV-35S promoter, in the vector. These localization experiments were performed using ubiquitin-driven constructs with a GFP-tag (pUBN::GFPN-MPK4). Recombined vectors were transformed in *A. tumefaciens* C58C1 strain which were subsequently infiltrated into *Nicotiana benthamiana* leaves, and GFP fluorescence was visualized after 3 d, essentially as described in Rayapuram *et al.* (2018).

### Pathogen assays

The virulent strain of *Pseudomonas syringae* pv *tomato*-DC3000 (Pst DC3000) was grown and maintained on LB agar plates at 28°C. The Pst DC3000 growth and inoculation procedure was carried out as described in Rayapuram & Baldwin (2008). In brief,  $1 \times 10^5$  cells  $\text{ml}^{-1}$  were resuspended in 0.1% Silwet L-77 solution and 4-wk-old *A. thaliana* plants were sprayed for 4 s. As a mock inoculation, leaves were sprayed with 0.1% Silwet L-77 solution. Sprayed plants were covered with a transparent plastic lid for the remaining time of the experiment. Bacterial titers were estimated 2 d postinfection (2 dpi). For bacterial titers, leaf disks from three different leaves per plant were harvested and surface-sterilized, and then bacteria were extracted using 10 mM  $\text{MgCl}_2$  containing 0.04% (v/v) Silwet L-77. Quantification was done by plating appropriate dilutions on LB agar media containing rifampicin (50  $\text{mg l}^{-1}$ ) and incubated at 28°C for 2 d, after which the bacterial colonies were counted.

### Methyl viologen-induced oxidative stress

Seeds were sterilized, stratified at 4°C for 3 d, and grown vertically on  $\frac{1}{2}$ MS solid medium (MS5524; Sigma) containing 0.5  $\text{g l}^{-1}$  MES, pH 5.7 and 1% (w/v) agar (A1296; Sigma), in a controlled chamber (22°C, 70% relative humidity, 16 h photoperiod at 100  $\mu\text{mol m}^{-2} \text{s}^{-1}$ ) for 14 d. Oxidative stress conditions were introduced adding 1 mM methyl viologen into the  $\frac{1}{2}$ MS medium to a final concentration of 50 nM. Root length and root density were measured at Day 14, while fresh weight measurements were performed after 4 wk.

### Protein extraction and western blots

Seedlings were ground into a fine powder with two metal beads using tissue lyser and homogenized in extraction buffer (50 mM Tris-HCl pH 7.5, 5 mM EDTA, 5 mM EGTA, 50 mM

$\beta$ -glycerophosphate, 10 mM sodium fluoride, 1 mM orthovanadate, 2 mM DTT, 1 $\times$  anti-protease cocktail; Roche). The supernatant was collected after centrifugation at 21 100 *g* for 15 min at 4°C. Protein concentration was determined with Bradford method, and all samples were adjusted to the same concentration before dilution with SDS-PAGE sample buffer. Total protein extracts (20  $\mu$ g) were separated on 10% SDS-polyacrylamide gels and immunoblotted onto polyvinylidene difluoride membranes (Millipore). Blots were blocked either with 5% (w/v) defatted milk (for anti-Cmyc and anti-MPK4 western blots) or 5% (w/v) BSA (for anti-pTpY western blot) in TBS-T (10 mM Tris-HCl, pH 7.5, 154 mM NaCl, 0.1% (v/v) Tween 20) and probed with 1 : 8000 anti-phospho-p44/42 MAPK (Erk1/2) (Thr202/Tyr204) (D13.14.4E) XP rabbit monoclonal antibody (#4370; Cell Signaling Technology, Danvers, MA, USA), 1 : 14 000 polyclonal anti-Cmyc antibodies (C3956; Sigma), or 1 : 10 000 anti-MPK4 (Nakagami *et al.*, 2006). Horseradish peroxidase-conjugated anti-rabbit IgG (Sigma) were used as secondary antibodies at 1 : 20 000, and the reactions were visualized with Clarity enhanced chemiluminescence ECL kit (Bio-Rad) using an imaging system (ChemiDoc MP System; Bio-Rad). Blots were stained with Coomassie blue for loading control. Western blots signals were quantified with IMAGE LAB software (Bio-Rad).

#### Cloning, expression, and purification of recombinant protein

The DNA fragments encoding full-length MPK4-FL and MPK4 residues 16–376 (MPK4 $\Delta$ 15) from *A. thaliana* were PCR-amplified with oligonucleotide primers (IDT, Leuven, Belgium; Table S2). The obtained fragments were digested with *Bam*HI and *Xho*I and ligated into an pGEX-6P-1 expression vector (GE Healthcare, Chicago, IL, USA). The MPK4 C181S and C181D mutants were generated by PCR according to Jeltsch & Lanio (2002) using primers (Table S2) designed to introduce the desired mutations into the pGEX-6P-1-MPK4 plasmid. After PCR, the mixture was digested with *Dpn*I and transformed into *E. coli* DH10 $\beta$  cells (Invitrogen) to generate the plasmid with the introduced mutation. All plasmids were verified by sequencing (KAUST Bioscience Core Lab, KAUST, Thuwal, Saudi Arabia). The plasmids were then transformed into *E. coli* BL21 (DE3) cells. Cells were grown in LB broth containing ampicillin (100 mg ml<sup>-1</sup>) at 37°C until an OD<sub>600</sub> of 0.6. Expression was induced by adding 200  $\mu$ M isopropyl  $\beta$ -D-1-thiogalactopyranoside (IPTG), and cultures were incubated at 16°C overnight. Cells were harvested by centrifugation at 8500 *g* for 10 min. The cell pellet from 1 l culture was resuspended in 30 ml of lysis buffer (50 mM Tris-HCl (pH 8.0), 200 mM NaCl, 3 mM DTT), and 0.1% Triton X-100 was added to it. The resuspended pellets were lysed by sonication. Cell debris was removed by centrifugation at 80 000 *g* for 30 min, and proteins were purified from the obtained supernatant using Glutathione Sepharose 4B resins (GE Healthcare; Shahul Hameed *et al.*, 2018). The N-terminal GST tag of MPK4 and mutants was removed by overnight incubation with PreScission Protease (GE Healthcare) at 4°C. After GST cleavage, proteins were

eluted with lysis buffer and further purified on a HiLoad16/60 Superdex 200 prep-grade gel filtration column (GE Healthcare) using a buffer containing 20 mM HEPES (pH 7.5), 150 mM NaCl, 3 mM DTT. Protein purity was evaluated using SDS-PAGE. The purified protein was concentrated to 10 mg ml<sup>-1</sup> and stored at -80°C.

#### *In vitro* kinase assays and phosphosite identification

The *in vitro* kinase assay and immunoprecipitation were performed as follows: Protein extracts (200  $\mu$ g) were incubated with 1  $\mu$ l polyclonal anti-Cmyc antibody (Sigma) in immunoprecipitation buffer (extraction buffer supplemented with 150 mM NaCl and 1% Triton X-100) for 2 h 30 at 4°C. Then, 20  $\mu$ l of 50% slurry Protein A-sepharose beads were added and the incubation was continued for another 1 h. The immunoprecipitates were washed three times in immunoprecipitation buffer and twice in protein kinase buffer (20 mM Tris-HCl pH 7.5, 5 mM EGTA, 10 mM MgCl<sub>2</sub>, 1 mM DTT). Then, the immunoprecipitates were incubated in reaction buffer (20 mM Tris-HCl pH 7.5, 5 mM EGTA, 10 mM MgCl<sub>2</sub>, 1 mM DTT, 50  $\mu$ M cold ATP, 2  $\mu$ Ci [ $\gamma$ -<sup>33</sup>P]ATP, 2  $\mu$ g maltose binding protein (MBP) substrate), at room temperature for 30 min. The reaction was stopped by adding SDS-PAGE loading buffer. Samples were heated at 95°C for 3 min and separated on 15% SDS-PAGE. Phosphorylation was detected on dried gels by the Typhoon imaging system (GE Healthcare). Gels were stained with Coomassie blue for loading control. Phosphorylation signals were quantified with IMAGEQUANT TL software (GE Healthcare) and normalized with MPK4-Cmyc protein level.

#### Isothermal titration calorimetry

Full-length MPK4, MPK4 C181D, MPK4 C181S, and MKK2 were dialyzed and degassed in isothermal titration calorimetry (ITC) buffer (20 mM HEPES pH 7.5, 150 mM NaCl, 3 mM DTT). High-purity MKK2 (1–19) peptide (MKKGGFSNNLKLAI PVAGE) was purchased from GenScript (Singapore) and dissolved in the identical buffer. For the MPK4 titrations with peptides, 20  $\mu$ M of recombinant MPK variants was placed in the cell, and 350  $\mu$ M of MKK2 peptide was loaded in the syringe. Titrations were performed at 25°C with an initial injection of 0.8  $\mu$ l, followed by 25 injections of 8  $\mu$ l. For the titrations of MPK4 with full-length MKK2, 20  $\mu$ M of MKK2 was kept in the cell and 300  $\mu$ M of MPK4 WT and mutants was injected from the syringe. Titrations were performed at 25°C with an initial injection of 0.5  $\mu$ l, followed by 40 injections of 5.5  $\mu$ l. ITC experiments were performed on Nano ITC (TA Instruments, New Castle, DE, USA). Data analysis was performed on NANOANALYTE software (New Castle, DE, USA).

#### Protein crystallization and structure determination

MPK4 $\Delta$ 15 was mixed with the synthetic peptide HER-RIIHRDLKPSNLLINH (derived from MKK1 positions 182–200) in a ratio of 1 : 1.5 of protein to peptides. Adenylyl-

imidodiphosphate (AMP-PNP) (Sigma) was added at a final concentration of 2 mM. The obtained protein complex was subjected to hanging drop vapor diffusion method for crystallization screening using commercially available sparse matrix screens. Cube-shaped crystals were obtained by equilibrating 1.0  $\mu\text{l}$  of protein complex (10 mg ml<sup>-1</sup>) with 1.0  $\mu\text{l}$  of reservoir solution (2% v/v Tacsimate<sup>TM</sup> pH 7.0, 100 mM HEPES pH 7.5 and 20% PEG 3350). The crystals appeared after 2 d at 23°C. For data collection, 25% glycerol was added to the well solution as a cryoprotectant, and the crystals were flash-cooled in liquid nitrogen. Data were collected at 100 K at the beamline Proxima 2A at the SOLEIL Synchrotron (Saint-Aubin, France), using a EIGER X 9M detector, respectively (proposal nos. 20150257, 20150957, 20160098). The data were processed in XDS. Initial phases were determined by molecular replacement using Balbes with the human ERK2 structure (PDB 2ERK) as search model. The structure was manually inspected and corrected using COOT and refined using PHENIX REFINER (Table S3). The figures were drawn with PYMOL.

### Protein modeling

Structural models for full-length MKK1 and MKK2 in complex with MPK4 were made by submitting the protein sequences to ALPHAFOLD (Jumper *et al.*, 2021), and the figures were drawn using PYMOL.

## Results

### Crystal structure of the MPK4-MKK1/2 docking motif complex

To experimentally confirm the presence of the CD domain in MPK4, and its importance for associating with MPK4 ligands, we set out to determine the crystallographic X-ray structure of MPK4. Recombinant and purified full-length MPK4 did not yield well-diffracting crystals. Therefore, we deleted the N-terminal 15 residues (which were predicted to be flexible) and produced the mutant MPK4 $\Delta$ 15. Apo MPK4 $\Delta$ 15 and MPK4 $\Delta$ 15 mixed with the docking motif of MKK2 also failed to crystallize. We conceived an artificial docking motif derived from the MKK1 sequence (HERRIHRDLKPSNLLINH, MKK1dock). In addition to the canonical docking motif (R/K-G-X- $\emptyset$ -X<sub>3-4</sub>- $\emptyset$ -X- $\emptyset$ , where  $\emptyset$  are hydrophobic residues) (Gaestel, 2015), this peptide had hydrophobic residues which we were hoping would facilitate protein-protein interactions in the crystal lattice. Indeed, MPK4 $\Delta$ 15-MKK1dock produced crystals diffracting up to 2.2 Å resolution in the presence of 2 mM of the nonhydrolysable ATP analog AMP-PNP. The crystallographic structure of MPK4 $\Delta$ 15 showed the canonical MAP kinase fold, with root-mean-square deviations of 1.28 and 0.97 Å to MPK6 and ERK2, respectively (Fig. 1a). Hence, despite being separated by *c.* 1 billion years of evolution, the human ERK2 was the closer structural match to MPK4 with the only significant difference being the extended activation loop in ERK2. Bound AMP-PNP was clearly defined in the electron density (Fig. S1a). Despite the

apparent absence of phosphorylation, the MPK4 activation loop residues were fairly well defined in the electron density (Fig. S1b). T201 and Y203 of the TEY motif and neighboring residues of V204 and R210 are oriented similarly to the doubly phosphorylated ERK2 activation loop (Fig. S1c; Canagarajah *et al.*, 1997). However, R210 did not bind to Y203 to form the so-called P + 1 site due to the lack of Y203 phosphorylation.

The MPK4 DFG motif was in the DFG-in position, suggesting that the kinase structure was partially mimicking its activated state. MKK1dock bound to a region on the C-terminal MPK4 lobe that corresponds to the CD domain in ERK2 (Tanoue *et al.*, 2000; Fig. 1b,c), validating that the CD domain-ligand interaction is conserved in MPK4. The hydrophobic residue L197 of MKK1dock that is not a part of the canonical docking site forms hydrophobic crystal contacts by interacting with L197 from a symmetry-related MKK1dock peptide. Additionally, the MKK1dock N199 side chain forms hydrogen bonds with the backbone carboxyl group of L196 from a symmetry-related MKK1dock (Fig. S2). These contacts would not be possible with the MKK2 peptide, explaining the failure of MKK2dock-MPK4 complexes to crystallize. These crystal contacts did not appear to significantly distort the MKK1dock peptide, because the crystallographic MKK1dock model superimposed well with the ALPHAFOLD-predicted position of the MKK2 docking motif bound to MPK4 (MKK2dock; residues 1–19; Figs 1d, S3, S4a).

### Role of MPK4 CD site in interaction with its upstream activating MAPKK (MKK1, MKK2, and MKK6)

Recently, *Arabidopsis* MPK4 was identified as an oxidation target in a hydrogen peroxide-dependent sulfenome screen of *Arabidopsis* cell cultures (Huang *et al.*, 2019). Amino acid sequence comparison of MPK4 with ERK2 indicated that the MPK4-C181 is conserved in human ERK2, corresponding to C161 and S-sulfenylation reduces ERK2 kinase activity (Keyes *et al.*, 2017). Moreover, Huang *et al.* (2019) showed that serine substitution of C181 (MPK4-C181S) resulted in a strong reduction of the MPK4 kinase activity *in vitro*, suggesting that C181 might play an important role in regulating the MPK4 pathway.

Our crystallographic structure showed that MPK4 C181 was situated in the center of the docking site, in direct contact with positions  $\emptyset$ -X- $\emptyset$  of the ligand peptide (P193 and L196 in MKK1dock; Fig. 1b,c). Structural modeling showed that the substitution of C181 with a serine would not impact ligand binding (Fig. S4b). However, *in silico* introduction of C181D led to clashes with MKK1dock and to an unfavorable proximity of the negative charge of D181 with the hydrophobic MKK1dock residues P193 and L196 (Fig. 1c). ALPHAFOLD models of MPK4 bound to the biologically relevant docking motifs from MKK1, MKK2, and MKK6 reproduced the clashes and proximity of D181 with the key hydrophobic residues of the docking motifs (Figs 1d, S4). These observations suggested that the MPK4 C181D variant is unable to bind docking motifs from upstream activators or downstream substrates.

To test whether the mutation at C181 in the D-site affects the interaction of MPK4 with its interaction partners, we assessed the

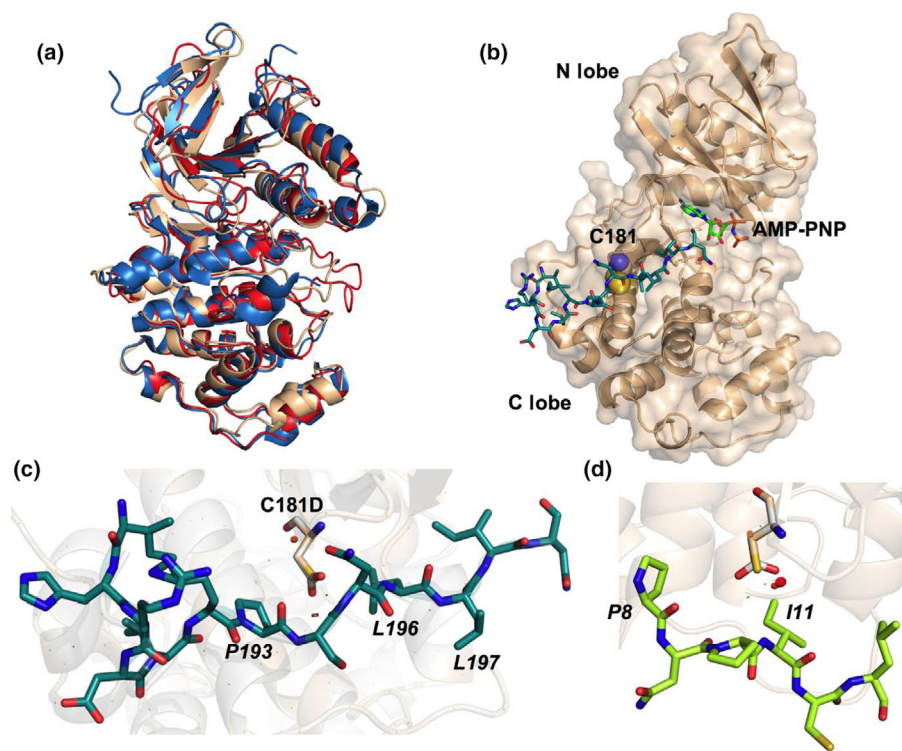


**Fig. 1** Crystal structure of Arabidopsis MPK4 bound to MKK1 dock peptide and adenylyl-imidodiphosphate (AMP-PNP). (a) Superimposition of MPK4 $\Delta$ 15 (light brown), human extracellular signal-related kinase2 (ERK2) (red; Protein Data Bank (PDB) accession no. 2ERK), and MPK6 (blue; PDB 6DTL) crystal structures. (b) Surface view and cartoon representation of MPK4 $\Delta$ 15 (light brown) bound to the MKK1 dock peptide (carbon atoms colored in teal) and AMP-PNP (green stick), C181 shown as a sphere. (c) Zoom on the interaction between MPK4-C181 (light brown stick) and MKK1 dock (teal). The *in silico* introduced C181D mutation (white stick), clashes (red disks) with MKK1 dock and leads to the unfavorable proximity between the negatively charged D181 from MPK4 and hydrophobic side chains (P193 and L166) from MKK1 dock. (d) The clashes and unfavorable proximity of the D181 charge with the docking motif are reproduced in an ALPHAFOLD model of MPK4 (light brown) bound to the biologically relevant MKK1 docking peptide (carbons are light green). C181D is colored as in (c).

interaction between MPK4 and commercially synthesized MKK2 dock. Isothermal titration calorimetry showed that MKK2 dock bound MPK4-C181 or MPK4-C181S with a dissociation constant ( $K_d$ ) of  $3.47 \pm 0.42$  and  $4.13 \pm 0.51$   $\mu$ M, respectively, in a 1:1 ratio. However, MPK4-C181D did not show binding to MKK2 dock (Fig. 2a–c; Table 1). We confirmed these observations using full-length MKK2 instead of its isolated docking peptide. ITC binding studies showed that MKK2 bound to MPK4-C181 or MPK4-C181S with  $K_{ds}$  of  $0.50 \pm 0.25$  and  $0.45 \pm 0.20$   $\mu$ M, respectively, in a 1:1 ratio, whereas MPK4-C181D failed to show binding to MKK2 (Fig. 2d–f; Table 1). These data clearly confirm that the CD domain–D-site interaction is essential also in the context of full-length MPK4 and MKK2. The slightly higher affinity observed with full-length proteins may result from weak additional contacts between MPK4 and MKK2, as suggested by structural ALPHAFOLD models (Fig. S3).

In summary, these data experimentally confirm the MKK2 D-site association and show that the C181D mutant of MPK4 is incapable of binding to D-site docking ligands because of a steric hindrance between the enlarged side chain at this position and the docking motif.

### Effects of MPK4 CD site modifications on plant phenotype

To unravel the role of the CD site of MPK4 on the plant phenotype and development *in vivo*, we generated stable transgenic lines expressing different MPK4 variants under the control of endogenous promoter in the *mpk4-2* genetic background: *mpk4-2::pMPK4::MPK4-C181* (complementation line), *mpk4-2::*

*pMPK4::MPK4-C181S* (oxidation insensitive), and *mpk4-2::pMPK4::MPK4-C181D* (putative oxidation mimic). *mpk4-2* mutants display dwarfism in shoots and in roots (Kosetsu *et al.*, 2010). By contrast, *mpk4-2::MPK4-C181S* lines exhibited a normal plant phenotype as Col-0 (WT) and *mpk4-2::MPK4-C181* (complementation) lines, implying that mutation at C181 into serine in the CD site has no effect under these conditions (Figs 3a,b, S5, S6). In comparison, *mpk4-2::MPK4-C181D* could not recover the dwarf phenotype with thick, short, serpentine-shaped roots of *mpk4-2*. This phenotype persisted throughout the entire life cycle, demonstrating the importance of the stereochemistry of the CD motif in plant growth.

To analyze phenotypic differences, we measured the fresh weight, primary root length, and lateral root density of all plant lines. The fresh weight of shoots and roots was reduced by 90% in *mpk4-2* and *mpk4-2::MPK4-C181D* lines compared with *mpk4-2::MPK4-C181S*, *mpk4-2::MPK4-C181* complementation and WT Col-0 plants (Fig. 4a,b). The dry weights displayed a similar trend (Fig. 4c,d), showing that *mpk4-2* and *mpk4-2::MPK4-C181D* plants are compromised in shoot and root growth.

To determine whether changes in the root architecture occurred, primary root length, and lateral root density of all plant lines were analyzed. The primary roots of WT Col-0, *mpk4-2::MPK4-C181*, and *mpk4-2::MPK4-C181S* were *c.* 8 cm long whereas those of *mpk4-2* and *mpk4-2::MPK4-C181D* were only *c.* 2 cm long, revealing a major reduction in primary root length by 75% (Fig. 4e). For lateral root density, we found *c.* 3 lateral roots  $\text{cm}^{-1}$  of primary root (Fig. 4f) in all plant lines, indicating that mutations in C181 did not affect this feature. In addition,

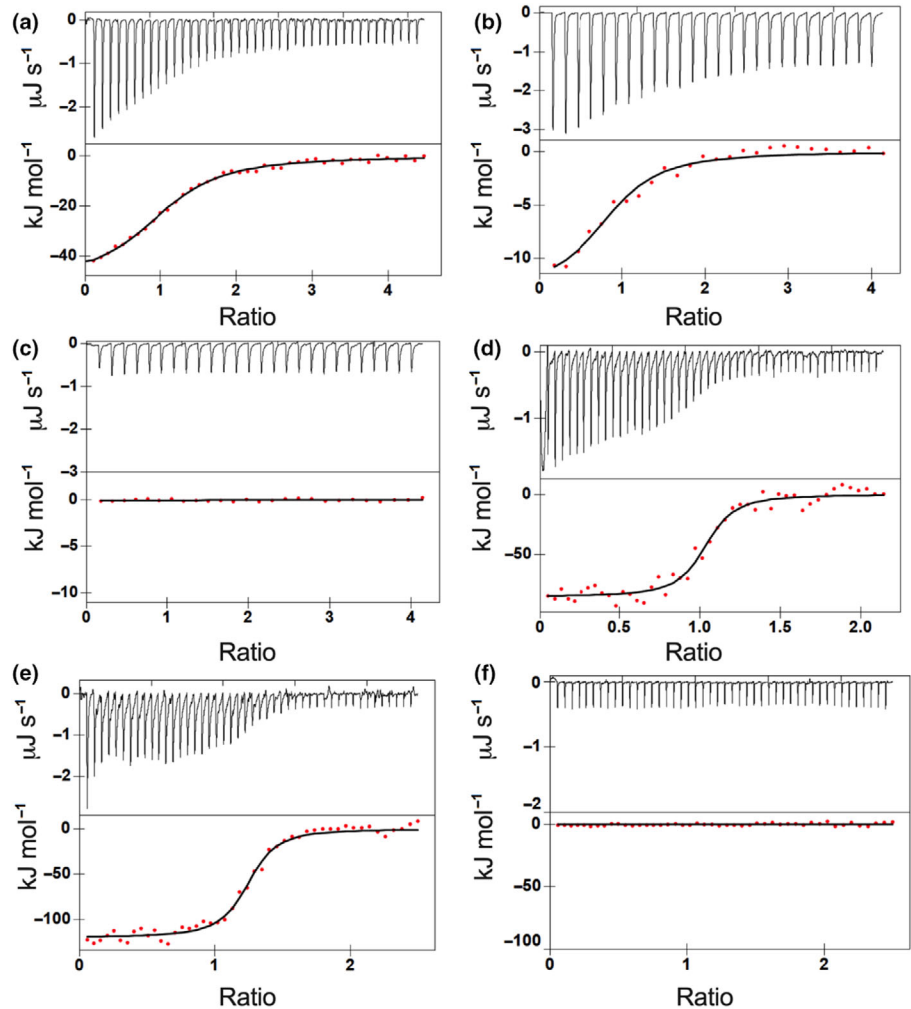


**Fig. 2** Interaction of Arabidopsis MKK2 D-site peptide or MKK2 full length (FL) with MPK4-C181, MPK4-C181S, and MPK4-C181D determined by isothermal titration calorimetry (ITC). MKK2 peptide interaction with (a) MPK4-C181, (b) MPK4-C181S, and (c) MPK4-C181D. MKK2 FL interaction with (d) MPK4-C181, (e) MPK4-C181S, and (f) MPK4-C181D. For each titration, the top panel shows the heats for each injection and the bottom panel shows the integrated heats, fitted by a sigmoid where appropriate.

**Table 1** Binding affinities of Arabidopsis MKK2 dock peptide and MKK2 FL MKK2 D-site peptide and MKK2 FL binding affinities toward MPK4-C181, MPK4-C181S, and MPK4-C181D, and the thermodynamic parameters derived from isothermal titration calorimetry (ITC) are shown (Fig. 2).

Sample in the cell	Sample in the syringe	N	$K_d$ ( $\mu\text{M}$ )	$\Delta G$ ( $\text{kJ mol}^{-1}$ )	$\Delta H$ ( $\text{kJ mol}^{-1}$ )	$T\Delta S$ ( $\text{kJ mol}^{-1} \text{K}^{-1}$ )
MPK4 C181	MKK2 D-site	$0.95 \pm 0.10$	$3.47 \pm 0.42$	$-31.17 \pm 4.25$	$-39.41 \pm 3.15$	$-8.24 \pm 1.25$
MPK4 C181S	MKK2 D-site	$0.93 \pm 0.15$	$4.13 \pm 0.51$	$-30.77 \pm 3.50$	$-13.05 \pm 0.97$	$17.72 \pm 2.25$
MPK4 C181D	MKK2 D-site	ND	NB	ND	ND	ND
MKK2 FL	MPK4 C181	$1.06 \pm 0.15$	$0.50 \pm 0.25$	$-38.06 \pm 4.15$	$-84.37 \pm 9.25$	$-46.31 \pm 5.25$
MKK2 FL	MPK4 C181S	$1.25 \pm 0.10$	$0.45 \pm 0.20$	$-36.87 \pm 3.75$	$-119.80 \pm 13.20$	$-82.93 \pm 10.30$
MKK2 FL	MPK4 C181D	ND	NB	ND	ND	ND

N, stoichiometry; NB, no binding; ND, not determined.

we investigated whether modification of C181 might affect MPK4 localization, which might alter MPK4 function. Analysis of *N. benthamiana* transiently expressing GFP-labeled MPK4-C181 variants did not show differences in MPK4 localization (Fig. S7).

The *mpk4-2* mutant phenotype also results from a disturbed microtubule organization and root cell plate formation (Beck *et al.*, 2010; Kosetsu *et al.*, 2010). Analysis of the cell division patterns in roots of *mpk4-2::MPK4-C181D* revealed an aberrant division pattern in root cells like in *mpk4-2* deficient plants.

*mpk4-2::MPK4-C181S*, however, displayed a normal division pattern (Fig. 3c). Collectively, our results demonstrate that the CD site of MPK4 is essential for proper Arabidopsis development.

#### Effects of MPK4 CD site mutations on seed maturation

The *mpk4-2* mutant is unable to produce viable seeds. This is due to defective male-specific meiotic cytokinesis (Zeng *et al.*, 2011) and premature synergid cell death (Völz *et al.*, 2022). We therefore assessed whether the CD side chain





**Fig. 3** Effects of Arabidopsis MPK4 common docking motif (CD) site mutations on plant phenotype. Phenotype of *Arabidopsis thaliana* WT, *mpk4-2*, *mpk4::pMPK4-MPK4-C181-PC2*, *mpk4::pMPK4-MPK4-C181S-PC2*, and *mpk4::pMPK4::MPK4-C181D-PC2* transgenic lines at different developmental stages. (a) Four-week-old soil-grown plants are shown. Bar, 1 cm. (b) Fourteen-day-old plants were cultivated on Murashige & Skoog basal medium under long-day conditions. Bar, 1 cm. (c) Root structure, red: propidium iodide dye marking cell walls. Bar, 50  $\mu$ m.

chemistry affects seed formation. Comparison of *mpk4-2::MPK4-C181D* and *mpk4-2::MPK4-C181S* lines with *mpk4-2* and WT Col-0 controls throughout their life cycle revealed the importance of C181 in seed maturation and production. The silique and seed formation in *mpk4-2::MPK4-C181S* was indistinguishable from WT plants (Fig. 5a–c). However, *mpk4-2::MPK4-C181D* siliques were smaller with a strongly reduced average number of seeds/silique, compared with WT and *mpk4-2::MPK4-C181S* plants (Fig. 5a–c). Interestingly, *c.* 30% of the *mpk4-2::MPK4-C181D* seeds reached maturity, while *c.* 70% of embryo sacs remained unfertilized (Fig. 5a–c). MPK4 is required for male-specific cytokinesis (Zeng *et al.*, 2011) and *mpk4* pollen cannot undergo normal male-meiotic cytokinesis, which results in bigger pollen grains with an increased number of sperm cells and vegetative cells. We found that the pollen diameter in *mpk4-2::MPK4-C181S* plants reflects WT pollen (Fig. 5d,e), but *mpk4-2::MPK4-C181D* plants showed an increased pollen diameter comparable to the previous findings in *mpk4* (Fig. 5d,e). We further raised the question of how the *MPK4-C181D* mutation affects plant reproduction, which prompted us to inspect the precursor structure of the seed, the embryo sac. The embryo sac

contains the haploid female gametophyte, which harbors two pollen tube-attracting synergids beside the egg and central cell, which give rise to the embryo and the embryo-nourishing tissue, called endosperm. The synergids degenerate after pollen tube reception and following the fertilization of egg and central cell (Völz & Groß-Hardt, 2010; Völz *et al.*, 2013). We found that formation of the egg and central cell was not broadly perturbed in *mpk4-2::MPK4-C181D* compared with WT and *mpk4-2::MPK4-C181S* plants. However, deep inspection of the *mpk4-2::MPK4-C181D* plants revealed a shortage of synergid cell number in the female gametophyte 48 h after emasculating of the oldest closed flower bud. The synergid formation in the *mpk4-2::MPK4-C181S* line was not affected and reminiscent to WT (Fig. 5f,g). These results revealed that CD site integrity is important for MPK4-dependent progression of male-cytokinesis and synergid formation.

### Role of MPK4 CD motif integrity in immunity

MPK4 suppresses plant resistance, and consequently, *mpk4* knockout mutants are more resistant toward the virulent strain *P. syringae* pv *tomato* (*Pst DC3000*) and *Peronospora parasitica* isolate Cala2 (Petersen *et al.*, 2000). To test whether the integrity of the CD site of MPK4 affects pathogen-associated molecular pattern (PAMP)-induced signaling, we investigated the effect of CD site mutants on plant defense against *Pst DC3000*. Treatment with *Pst DC3000* showed that *mpk4-2* and *mpk4-2::MPK4-C181D* plants were more resistant compared with WT, *mpk4-2::MPK4-C181* *mpk4-2*, and *mpk4-2::MPK4-C181S* plants (Fig. 6). The number of bacteria per mg of plant weight in *mpk4-2* and *mpk4-2::MPK4-C181D* plants was reduced by > 20-fold when compared to Col-0, *mpk4-2::MPK4-C181S*, and *mpk4-2::MPK4-C181* lines. These results show that the CD site of MPK4 is critical for the resistance toward the bacterial pathogen *Pst DC3000*.

### Role of MPK4 CD motif integrity in abiotic stress resistance

C181S cannot be sulfenylated and hence can be expected to react differently to oxidative stress conditions *in vivo*. Thus, plants were treated with methyl viologen (MV), which is a herbicide and can induce light-dependent ROS production. In plants, light energy is normally transmitted in chloroplasts by ferredoxin of photosystem I, but MV acts as a competitor to ferredoxin, thereby capturing and passing electrons over to O<sub>2</sub> to generate superoxide, which is subsequently converted to hydrogen peroxide (Babbs *et al.*, 1989).

Methyl viologen- and mock-treated plants were analyzed for fresh and dry weight and root phenotypes. *mpk4-2* mutants and *mpk4-2::MPK4-C181D* plants were more resistant toward MV-induced oxidative stress, compared with *mpk4-2::MPK4-C181S* which behaved as WT and *mpk4-2::MPK4-C181* complementation lines with respect to primary root length (Fig. 7a,b). WT, complementation and *MPK4-C181S mpk4-2* plants exhibited a similar reduction in fresh weight of shoots (53%) as in roots (15%) compared with *mpk4-2* and *mpk4-2::MPK4-C181D* (Fig. 7e,f). *mpk4-2::*

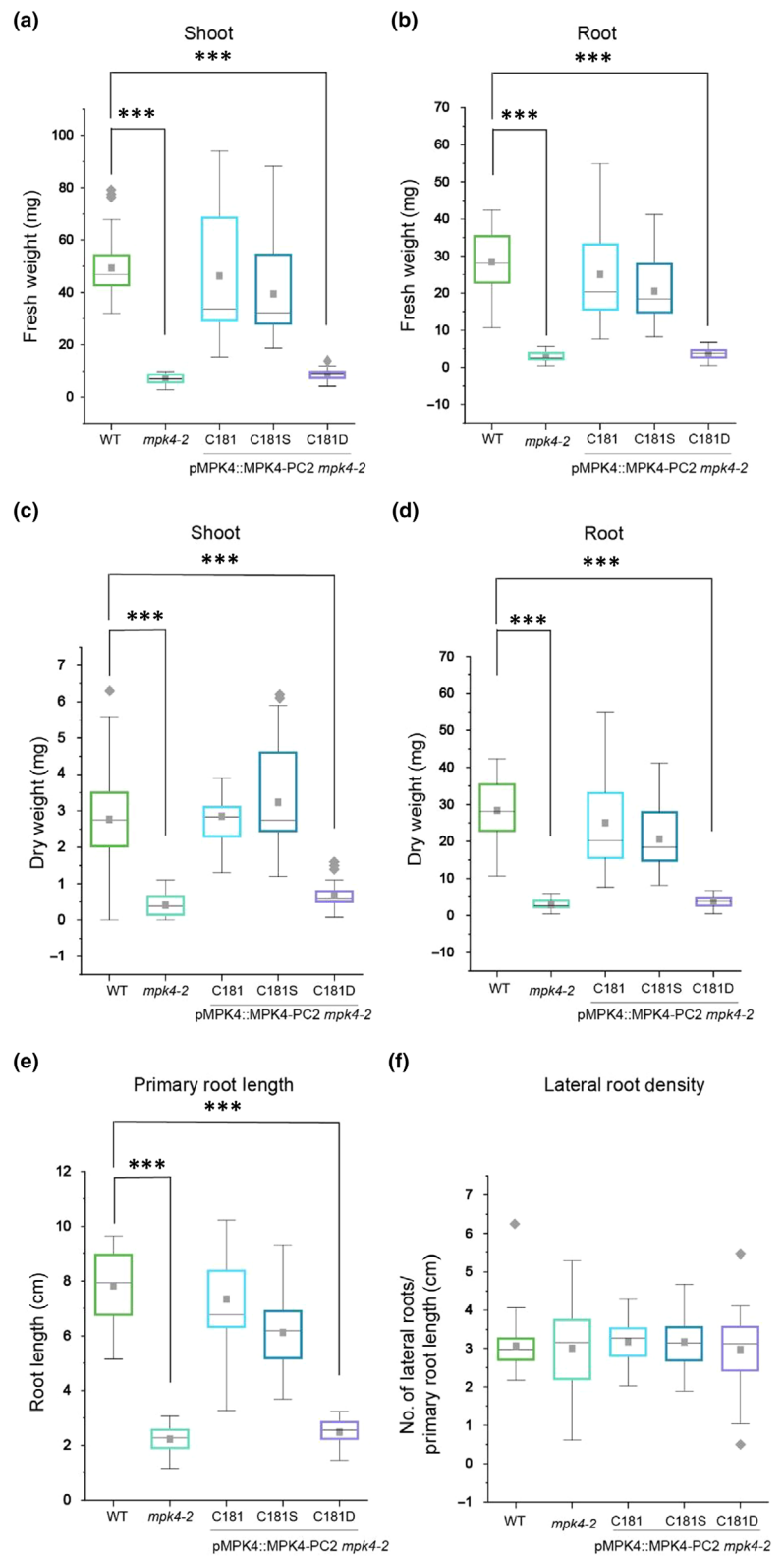


**Fig. 4** Effects of Arabidopsis MPK4 common docking motif (CD) site modifications on plant growth and development. Plant fresh weight and dry weight of *Arabidopsis* seedlings grown on 1/2-strength Murashige & Skoog medium (1/2MS). The data for fresh weight (a, b), dry weight (c, d), primary root length (e), and lateral root density (f) were measured at Day 14. Asterisks indicate significant differences by *t*-test at  $P \leq 0.05$ . The center line in the box plot represents to the median, the box limits represents to the upper and lower quartiles and the whiskers denote  $1.5 \times$  interquartile range. Statistical significance is indicated in the graphs based on *t*-test (\*\*\*,  $P < 0.001$ ).

*MPK4-C181D* and *mpk4-2* showed significantly lower accumulation of anthocyanins than WT, *mpk4-2::MPK4-C181* complementation, and *mpk4-2::MPK4-C181S* lines (Fig. 7g). These results show an important role of the CD site of MPK4 in oxidative stress.

#### Effects of MPK4 CD site modifications on MAPK activity

MAPKs show low autoactivity *in vitro* but can be strongly activated by their respective upstream MAPKKs under stress conditions (Colcombet & Hirt, 2008). Knockout mutants of *mpk4*

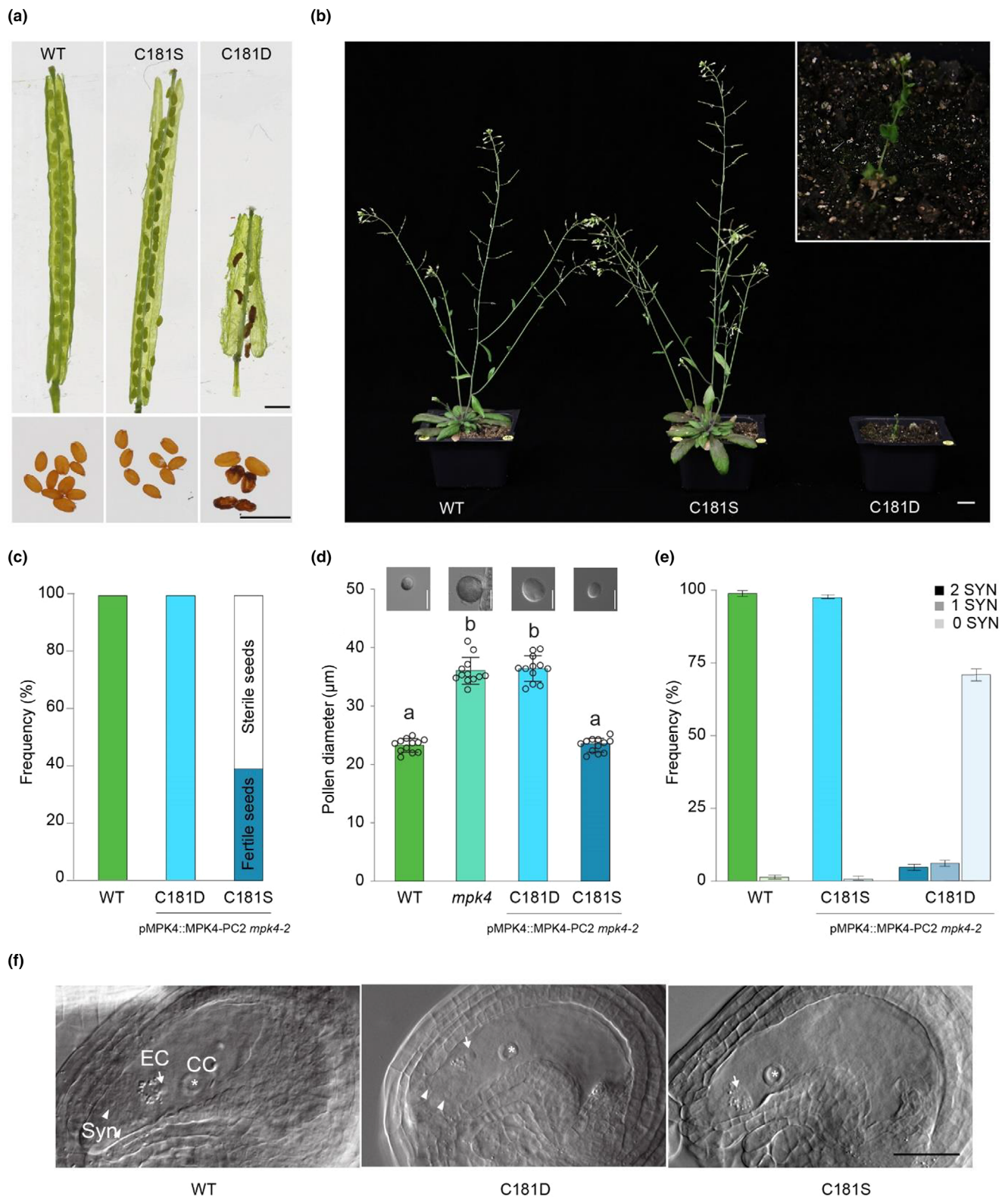


**Fig. 5** Effects of Arabidopsis *MPK4* CD site mutations on seed production and synergid formation. (a) Representative images of the seed set in the siliques and respective seeds of *MPK4-C181*, *MPK4-C181D*, and *MPK4-C181S* plants. Bar, 1 mm. (b) Representative image of *MPK4-C181*, *MPK4-C181S*, and *MPK4-C181D* mutant plants. Bar, 1 mm. (c) Seed formation in *MPK4-C181* ( $n = 2$ ), *MPK4-C181D* ( $n = 64$ ) and *MPK4-C181S* ( $n = 2$ ) and image of isolated seeds from respective plants. (d) Pollen diameter of *MPK4-C181*, *MPK4-C181S* and *MPK4-C181D* and *mpk4-2* pollen. Differential interference contrast microscopy of *MPK4-C181*, *MPK4-C181S*, and *MPK4-C181D* pollen. Bars, 30  $\mu\text{m}$ . (e) Frequency of synergids in ovules of *MPK4-C181* ( $n = 97$ ), *MPK4-C181D* ( $n = 82$ ), and *MPK4-C181S* lines ( $n = 98$ ). (f) Differential interference contrast microscopy of *MPK4-C181*, *MPK4-C181S*, and *MPK4-C181D* female gametophytes. White arrowhead, synergid (Syn); white arrow, egg cell (EC); white asterisk, central cell nucleus (CC). Bar, 30  $\mu\text{m}$ . Lowercase letters indicate significant differences between treatments ( $P < 0.05$ ). Different lowercase letters indicate significant difference at the 5% level.

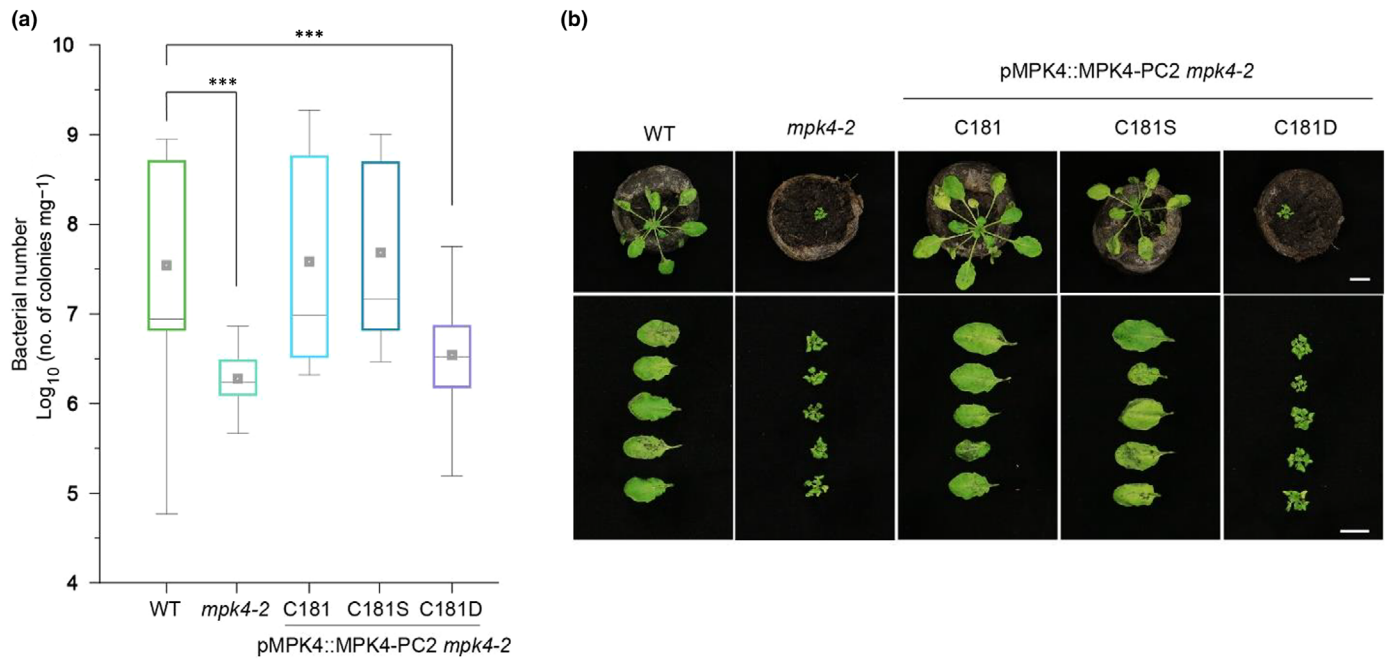


**Fig. 6** Role of Arabidopsis MPK4 common docking motif (CD) site on resistance toward *Pst* DC3000. (a) *Pst* DC3000 bacterial growth was evaluated at 2 d postinfection (dpi). *Pst* DC3000 pathogen assay results are an average of three biological replicates each consisting of nine leaf disks ( $n = 27$ ). Asterisks indicate significant differences by *t*-test at  $P \leq 0.05$ . (b) Disease symptoms in Col-0, *mpk4-2*, *MPK4-C181*, *MPK4-C181S*, and *MPK4-C181D* lines. Four-week-old plants were spray-inoculated with  $10^6$  CFU ml<sup>-1</sup>. Pictures were taken 2 dpi. Bars, 1 cm. The center line in the box plot represents to the median, the box limits represents to the upper and lower quartiles and the whiskers denote 1.5 $\times$  interquartile range. Statistical significance is indicated in the graphs based on *t*-test (\*\*\*,  $P < 0.001$ ).

show strong phenotypes with respect to development, but it is not clear whether the presence or the activation of MPK4 kinase by upstream MAPKKs is necessary for allowing normal development. The work by Huang *et al.* (2019) showed that serine substitution of C181 (MPK4-C181S) in the CD motif compromises MPK4 kinase activity. These assays were carried out *in vitro*, using the artificial substrate myelin basic protein, which does not possess a MAPK docking motif, and in the absence of the upstream activating MAPKKs. To overcome these shortcomings, it was important to investigate the MAP kinase activities of the MPK4-C181 variants *in vivo* under basal conditions and upon flg22 treatment for activation of MPK4 by its upstream MAPKKs. We therefore immunoprecipitated the different MPK4-PC2 proteins with anti-Cmyc antibody from *mpk4-2::MPK4-C181D*, *mpk4-2::MPK4-C181S*, and *mpk4-2::MPK4-C181* (complementation) lines, using Col-0 and *mpk4-2* lines as controls (Fig. 8). As judged from MBP phosphorylation levels as readout of MAPK activity, MPK4 kinase activity was significantly reduced in *mpk4-2::MPK4-C181D* (Fig. 7a, MPK4-Cmyc activity). Because MPK4-Cmyc expression levels vary to some extent between different lines (Fig. 8a, WB  $\alpha$ -Cmyc), MAPK activity signals were normalized to MPK4-Cmyc expression levels (Fig. 8b), revealing that upon flg22 treatment MPK4-C181D has strongly reduced kinase activity, while MPK4-C181S behaved like MPK4-C181. Next, we investigated whether the reduced MPK4 kinase activity was due to reduced phosphorylation of MPK4 by its upstream activating MAPKKs. For this, the protein samples were analyzed by western blotting with an antibody raised against the dual phosphorylated TEY motif of the MPK4

activation loop in activated MAPKs (Fig. 8a, WB  $\alpha$ -pTEpY). The signals were quantified and normalized to the respective MPK4-Cmyc expression levels (Fig. 8c). These experiments were repeated with independently generated *mpk4-2::MPK4-C181*, *mpk4-2::MPK4-C181S*, and *mpk4-2::MPK4-C181* lines (Fig. S8), confirming that CD site integrity is essential for TEY phosphorylation and MAP kinase activity.

Flg22 induces a defense mechanism in *Arabidopsis* plants that also includes the activation of MPK3 and MPK6. Therefore, we analyzed the phosphorylation status of MPK3 and MPK6 by western blots (Fig. 8a, WB  $\alpha$ -pTEpY). The anti-pTEpY antibody detected the enhanced phosphorylation of the endogenous MAPKs in all lines upon flg22 treatment. An increase in MPK3 and MPK6 phosphorylation levels was observed in *mpk4-2* and *mpk4-2::MPK4-C181D* but not in *mpk4-2::MPK4-C181* or *mpk4-2::MPK4-C181S* lines (Figs 8a,d, S8a,d). These results confirm that MPK4 is a negative regulator of MPK3 and MPK6 (Frei Dit Frey *et al.*, 2014).

Overall, these data show that the CD site of MPK4 plays a key role in its phosphorylation and associated MAP kinase activity during normal development and upon PAMP activation.

## Discussion

The function of plant MAPKs generally depends on their TEY phosphorylation status of their activation loop. For phosphorylation of MAPKs to occur, the D-site of an activating MAPK kinase has to specifically interact with the CD domain of the respectively targeted MAPK. Despite

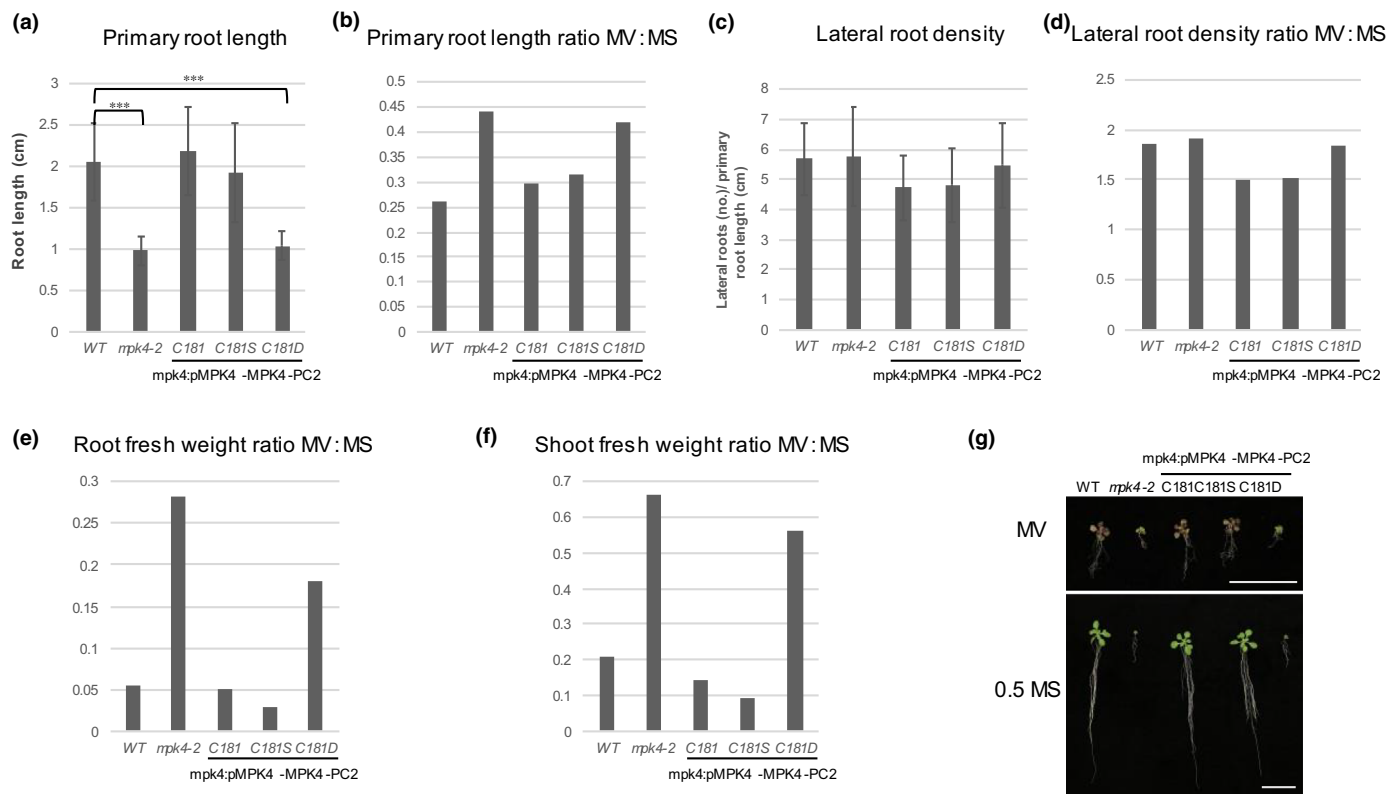


**Fig. 7** Role of Arabidopsis MPK4 common docking motif (CD) site integrity on oxidative stress resistance. Methyl viologen (MV) treatment on *Arabidopsis thaliana* WT, *mpk4-2* mutant and *mpk4:pMPK4-MPK4-C181*, *mpk4:pMPK4-MPK4-C181S*, and *mpk4:pMPK4:MPK4-C181D* transgenic lines. The data for primary root length (a, b) and lateral root density (c, d) were measured at Day 14 ( $n = 36$ ). Ratios of methyl viologen- to mock-treated primary root length (b), lateral root density (d) at Day 14 as well as for root (e) and shoot fresh weight (f) which were measured from 4-wk-old plants. Asterisks indicate significant differences by  $t$ -test at  $P \leq 0.05$ . Methyl viologen :  $\frac{1}{2}$ -strength Murashige & Skoog medium ( $\frac{1}{2}$ MS) ratios display the changes between both conditions. (g) Col-0, *mpk4-2*, *MPK4-C181*, *MPK4-C181S*, and *MPK4-C181D* lines grown on  $\frac{1}{2}$ MS or  $\frac{1}{2}$ MS with added to MV. Four-week-old plants. Bars, 1 cm. Statistical significance is indicated in the graphs based on  $t$ -test (\*\*\*,  $P < 0.001$ ).

compelling evidence for this mechanism in animal MAPKs, little is yet known how important these motifs are in plant MAPK signaling pathways. Our crystallographic data of the MPK4-MKK1dock motif complex provide the basis for a molecular understanding that an intact plant MAPK CD motif is essential for interaction with upstream MAPKs. We also provide evidence that single amino acid modifications in the CD motif of MAPKs can have severe consequences for MAPK activation and functionality *in vivo*.

MAPK activation by MAPKs and inactivation by MAPK phosphatases has been studied extensively in many systems and shows that the pTEpY phosphorylation status of the activation loop is of outstanding importance for MAPK activity. However, MAPK activity can also be influenced by other post-translational mechanisms. For example, acetylation within the ATP-binding pocket of the human MAPK p38 $\alpha$  promotes the affinity of the MAPK toward ATP (Pillai *et al.*, 2011). Phosphorylation on T123, which is located in the docking groove, negatively affects p38 $\alpha$ 's binding ability for MKKs (Peregrin *et al.*, 2006). Another post-translational modification on p38 $\alpha$  is methylation of the two arginines R49 and R149. Nonmethylated p38 $\alpha$  shows reduced binding activity to its upstream activating kinase MKK3 and to its downstream effector MAPKAPK2. In addition,

MKK3-induced p38 $\alpha$  activation is greatly reduced in nonmethylated mutants (Liu *et al.*, 2020).

Multiple evidence also indicates a role of MAPKs in oxidative signaling and stress responses of plants. H<sub>2</sub>O<sub>2</sub> activates MAPK pathways via MAPKKs, as shown for OMTK1 and MEKK1 (Nakagami *et al.*, 2004). *MEKK1*-deficient plants show elevated ROS levels and deregulation of genes involved in cellular redox control, similar to *mpk4* mutants (Nakagami *et al.*, 2006). Moreover, the activity of MEKK1 is controlled by H<sub>2</sub>O<sub>2</sub> in a proteasome-dependent manner and *mekk1* mutants exhibit reduced ROS-induced MPK4 activation (Nakagami *et al.*, 2006). Since serine-substituted C181 of Arabidopsis MPK4 was reported to be compromising the MAP kinase activity *in vitro* (Huang *et al.*, 2019), ROS regulation of the MPK4-targeted autoimmunity phenotype by SUMM2 and SMN1 might be an attractive mechanism for regulating growth and defense. However, our data demonstrate that the nonsulfenylatable MPK4-C181S protein does not possess less kinase activity than WT MPK4-C181 (Fig. 8). Moreover, MPK4-C181S fully complements the growth, developmental, and immunity-related phenotypes of *mpk4-2* knockout mutant plants under all conditions. These results do not support an important role of MPK4-C181 sulfenylation in these processes.

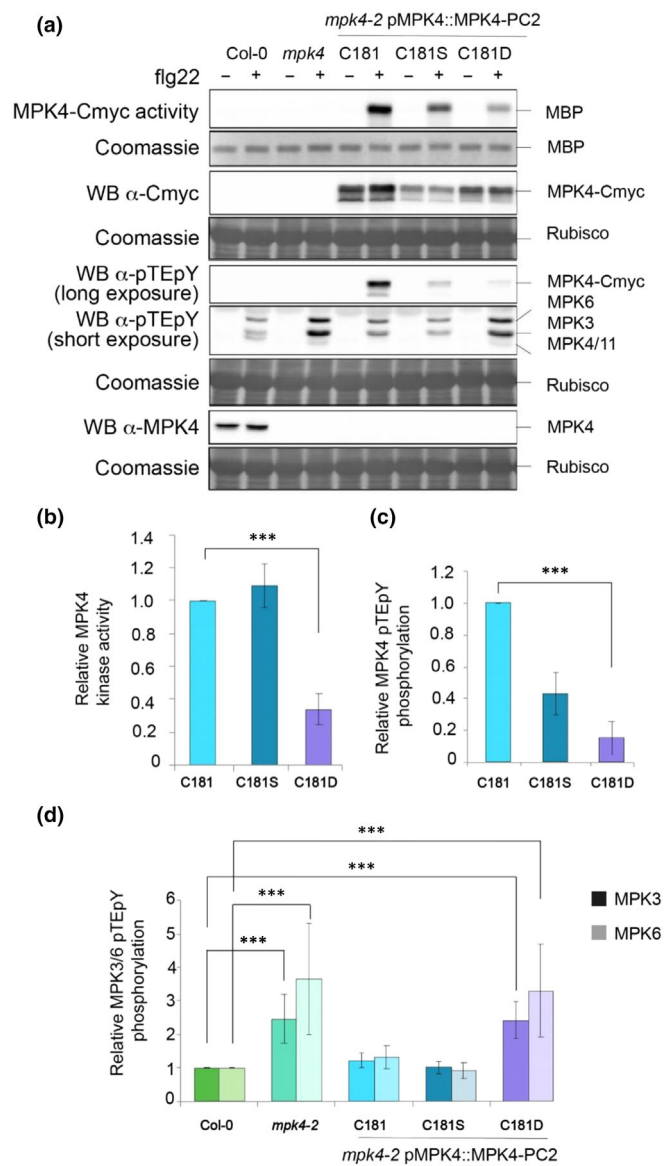


**Fig. 8** Role of Arabidopsis MPK4 common docking motif (CD) domain on mitogen-activated protein (MAP) kinase activity. (a) Activity, phosphorylation, and expression of MPK4-PC2 variants, as well as endogenous mitogen-activated protein kinases (MAPKs), in transgenic lines. MPK4-PC2 activity was measured on maltose binding protein (MBP) as substrate, after immunoprecipitation with anti-Cmyc antibody from seedlings treated with mock (–) or 1  $\mu$ M flg22 (+) for 15 min. Protein loading was controlled by Coomassie staining (MBP). Western blots were performed on the same protein samples before immunoprecipitation. MPK4-Cmyc and MPK4 expression levels were monitored by western blotting with anti-Cmyc and anti-MPK4, respectively. pTpY-phosphorylation levels were monitored by western blotting with anti-pTpY antibody. Protein loading was controlled by Coomassie staining. (b, c) Quantification of (b) MPK4-Cmyc kinase activity and (c) MPK4-Cmyc pTpY-phosphorylation levels. Western blot signals in (a) were quantified, normalized with MPK4 protein levels, and expressed relatively to MPK4-C181. Data are means  $\pm$  SD of three independent biological replicates. Asterisks indicate statistical difference from MPK4-C181 (Kruskal–Wallis test:  $P < 0.05$ ). (d) Quantification of MPK3 and MPK6 pTpY-phosphorylation levels. Western blot signals in A were quantified, normalized with protein loading, and expressed relatively to WT. Data are means  $\pm$  SD of three independent biological replicates. Asterisks indicate statistical difference from WT (Kruskal–Wallis test:  $P < 0.05$ ). Statistical significance is indicated in the graphs based on  $t$ -test (\*\*\*,  $P < 0.001$ ).

It might be argued that oxidation of cysteines can not only result in sulfenylation but also in persulfidation in a process of converting a mercapto group (Cys-SH) of the amino acid cysteine into hydropersulfide groups (Cys-SSH), via the intermediary oxidation into sulfenic acid (Zhang *et al.*, 2021). Persulfidation also plays an important role during PTI (Siodmak & Hirt, 2021). For instance, persulfidation of RBOHD affects its activity and the cellular ROS status (Zhang *et al.*, 2020), implying complex regulatory mechanisms that integrate different types of cysteine modifications. Based on our structural analysis, if persulfidation of MPK4-C181 occurs, it is expected to induce similar steric hindrance effects as observed for MPK4-C181D.

C181 was substituted by aspartic acid in MPK4 to give MPK4-C181D. The crystal structure and *in vitro* interaction studies confirm that C181D sterically hinders the CD site of MPK4 to interact with its activating MAPKK. Consequently, activation of MPK4-C181D by phosphorylation in the TEY site of its activation loop is not possible by upstream MAPKKs, rendering MPK4-C181D a constitutively inactive kinase. MPK4-C181D allows the possibility to study the question whether an inactive MPK4 protein suffices to maintain functioning of MPK4 in the context of development or stress signaling. Our analysis of *MPK4-C181D* clearly shows that an inactive MPK4 cannot substitute a knockout *mpk4-2* mutant. These results indicate that an activatable MPK4 is essential for functioning of the MAPK in development and stress signaling.

## Acknowledgements

We acknowledge SOLEIL for provision of synchrotron radiation facilities, and we would like to thank L. Chavas, P. Legrand, S. Sirigu, and P. Montaville for assistance in using beamline PROXIMA 1; G. Fox, M. Savko, and B. Shepard for assistance in using beamline PROXIMA 2A; and J. Perez and A. Thureau for assistance in using the beamline SWING. We would like to thank the KAUST Bioscience Corelabs for technical assistance for proteomics analysis and all members of the Hirt laboratory. For computer time, this research used the resources of the Supercomputing Laboratory at King Abdullah University of Science & Technology (KAUST) in Thuwal, Saudi Arabia. This publication is based on work supported by King Abdullah University of Science and Technology (KAUST) through the baseline fund to HH (BAS/1/1062-01-01) and STA (BAS/1/1056-01-01) and the Award no. URF/1/2965-01 from the Office of Sponsored Research (OSR).

## Competing interests










None declared.

## Author contributions

AS, UFSH, STA, NR and HH designed the study. AS, UFSH, NR, RV, MB, SA, HA, Y-HL, IB and STA performed the experimental work. AS, UFSH, STA and NR performed *in silico*

analysis and analyzed data. AS, UFSH, STA, NR and HH wrote the manuscript. All authors read and approved the manuscript. AS and UFSH contributed equally to this work.

## ORCID

Stefan T. Arold  <https://orcid.org/0000-0001-5278-0668>  
Ikram Blilou  <https://orcid.org/0000-0001-8003-3782>  
Marie Boudsocq  <https://orcid.org/0000-0001-8945-6773>  
Heribert Hirt  <https://orcid.org/0000-0003-3119-9633>  
Yong-Hwan Lee  <https://orcid.org/0000-0003-2462-1250>  
Naganand Rayapuram  <https://orcid.org/0000-0003-2056-3735>  
Umar F. Shahul Hameed  <https://orcid.org/0000-0002-0552-7149>  
Anna Siodmak  <https://orcid.org/0000-0001-8067-0407>  
Ronny Völz  <https://orcid.org/0000-0002-5385-0100>

## Data availability

The accession numbers for crystallographic data and models for MPK4 (16–376) + MKK1 dock peptide is 7W5C.

## References

- Babbs CF, Pham JA, Coolbaugh RC. 1989. Lethal hydroxyl radical production in paraquat-treated plants. *Plant Physiology* **90**: 1267–1270.
- Bardwell L. 2006. Mechanisms of MAPK signalling specificity. *Biochemical Society Transactions* **34**(Pt 5): 837–841.
- Beck M, Komis G, Müller J, Menzel D, Šamaj J. 2010. Arabidopsis homologs of nucleus- and phragmoplast-localized kinase 2 and 3 and mitogen-activated protein kinase 4 are essential for microtubule organization. *Plant Cell* **22**: 755–771.
- Bigeard J, Colcombet J, Hirt H. 2015. Signaling mechanisms in pattern-triggered immunity (PTI). *Molecular Plant* **8**: 521–539.
- Canagarajah BJ, Khokhlatchev A, Cobb MH, Goldsmith EJ. 1997. Activation mechanism of the MAP kinase ERK2 by dual phosphorylation. *Cell* **90**: 859–869.
- Colcombet J, Hirt H. 2008. Arabidopsis MAPK pathways: a complex signalling network involved in multiple biological processes. *Biochemical Journal* **413**: 217–226.
- Dorin D, Alano P, Boccaccio I, Cicerón L, Doerig C, Sulpice R, Parzy D, Doerig C. 1999. An atypical mitogen-activated protein kinase (MAPK) homologue expressed in gametocytes of the human malaria parasite *Plasmodium falciparum*. Identification of a MAPK signature. *Journal of Biological Chemistry* **274**: 29912–29920.
- Du X, Jin Z, Liu D, Yang G, Pei Y. 2017. Hydrogen sulfide alleviates the cold stress through MPK4 in *Arabidopsis thaliana*. *Plant Physiology and Biochemistry* **120**: 112–119.
- Edwards K, Johnstone C, Thompson C. 1991. A simple and rapid method for the preparation of plant genomic DNA for PCR analysis. *Nucleic Acids Research* **19**: 1349.
- Frei Dit Frey N, Garcia AV, Bigeard J, Zaag R, Bueso E, Garmier M, Pateyron S, de Tauzia-Moreau ML, Brunaud V, Balzergue S *et al.* 2014. Functional analysis of Arabidopsis immune-related MAPKs uncovers a role for MPK3 as negative regulator of inducible defences. *Genome Biology* **15**: R87.
- Gaestel M. 2015. MAPK-activated protein kinases (MKs): novel insights and challenges. *Frontiers in Cell and Development Biology* **3**: 88.
- Gao M, Liu J, Bi D, Zhang Z, Cheng F, Chen S, Zhang Y. 2008. MEKK1, MKK1/MKK2 and MPK4 function together in a mitogen-activated protein kinase cascade to regulate innate immunity in plants. *Cell Research* **18**: 1190–1198.
- Gawroński P, Witoń D, Vashutina K, Bederska M, Betliński B, Rusaczonek A, Karpiński S. 2014. Mitogen-activated protein kinase 4 is a salicylic acid-independent regulator of growth but not of photosynthesis in Arabidopsis. *Molecular Plant* **7**: 1151–1166.
- Huang J, Willems P, Wei B, Tian C, Ferreira RB, Bodra N, Martínez Gache SA, Wahni K, Liu K, Vertommen D *et al.* 2019. Mining for protein S-sulfenylation in Arabidopsis uncovers redox-sensitive sites. *Proceedings of the National Academy of Sciences, USA* **116**: 21256–21261.
- Ichimura K, Casais C, Peck SC, Shinozaki K, Shirasu K. 2006. MEKK1 is required for MPK4 activation and regulates tissue-specific and temperature-dependent cell death in Arabidopsis. *Journal of Biological Chemistry* **281**: 36969–36976.
- Jeltsch A, Lanio T. 2002. Site-directed mutagenesis by polymerase chain reaction. In: Braman J, ed. *In vitro mutagenesis protocols. Methods in molecular biology*<sup>TM</sup>, vol. 182. Totowa, NJ, USA: Humana Press, 85–94.
- Jumper J, Evans R, Pritzel A, Green T, Figurnov M, Ronneberger O, Tunyasuvunakool K, Bates R, Židek A, Potapenko A *et al.* 2021. Highly accurate protein structure prediction with ALPHAFOLD. *Nature* **596**: 583–589.
- Keyes JD, Parsonage D, Yammani RD, Rogers LC, Kesty C, Furdui CM, Nelson KJ, Poole LB. 2017. Endogenous, regulatory cysteine sulfenylation of ERK kinases in response to proliferative signals. *Free Radical Biology & Medicine* **112**: 534–543.
- Kosetsu K, Matsunaga S, Nakagami H, Colcombet J, Sasabe M, Soyano T, Takahashi Y, Hirt H, Machida Y. 2010. The MAP kinase MPK4 is required for cytokinesis in *Arabidopsis thaliana*. *Plant Cell* **22**: 3778–3790.
- Lian K, Gao F, Sun T, van Wersch R, Ao K, Kong Q, Nitta Y, Wu D, Krysan P, Zhang Y. 2018. MKK6 functions in two parallel MAP kinase cascades in immune signaling. *Plant Physiology* **178**: 1284–1295.
- Liu MY, Hua WK, Chen CJ, Lin WJ. 2020. The MKK-dependent phosphorylation of p38 $\alpha$  is augmented by arginine methylation on Arg49/Arg149 during erythroid differentiation. *International Journal of Molecular Sciences* **21**: 3546.
- Nakagami H, Kiegerl S, Hirt H. 2004. OMTK1, a novel MAPKKK, channels oxidative stress signaling through direct MAPK interaction. *Journal of Biological Chemistry* **279**: 26959–26966.
- Nakagami H, Soukupová H, Schikora A, Zárský V, Hirt H. 2006. A mitogen-activated protein kinase kinase mediates reactive oxygen species homeostasis in Arabidopsis. *Journal of Biological Chemistry* **281**: 38697–38704.
- Peregrin S, Jurado-Pueyo M, Campos PM, Sanz-Moreno V, Ruiz-Gomez A, Crespo P, Mayor F Jr, Murga C. 2006. Phosphorylation of p38 by GRK2 at the docking groove unveils a novel mechanism for inactivating p38MAPK. *Current Biology* **16**: 2042–2047.
- Petersen M, Brodersen P, Naested H, Andreasson E, Lindhart U, Johansen B, Nielsen HB, Lacy M, Austin MJ, Parker JE *et al.* 2000. Arabidopsis map kinase 4 negatively regulates systemic acquired resistance. *Cell* **103**: 1111–1120.
- Pillai VB, Sundaresan NR, Samant SA, Wolfgeher D, Trivedi CM, Gupta MP. 2011. Acetylation of a conserved lysine residue in the ATP binding pocket of p38 augments its kinase activity during hypertrophy of cardiomyocytes. *Molecular and Cellular Biology* **31**: 2349–2363.
- Pitzschke A, Djamei A, Bitton F, Hirt H. 2009. A major role of the MEKK1-MKK1/2-MPK4 pathway in ROS signalling. *Molecular Plant* **2**: 120–137.
- Rayapuram C, Baldwin IT. 2008. Host-plant-mediated effects of Nadenfensin on herbivore and pathogen resistance in *Nicotiana attenuata*. *BMC Plant Biology* **8**: 109.
- Rayapuram N, Bigeard J, Alhoraibi H, Bonhomme L, Hesse AM, Vinh J, Hirt H, Pflieger D. 2018. Quantitative phosphoproteomic analysis reveals shared and specific targets of Arabidopsis mitogen-activated protein kinases (MAPKs) MPK3, MPK4, and MPK6. *Molecular & Cellular Proteomics* **17**: 61–80.
- Rayapuram N, Bonhomme L, Bigeard J, Haddadou K, Przybylski C, Hirt H, Pflieger D. 2014. Identification of novel PAMP-triggered phosphorylation and dephosphorylation events in *Arabidopsis thaliana* by quantitative phosphoproteomic analysis. *Journal of Proteome Research* **13**: 2137–2151.
- Shahul Hameed U, Haider I, Jamil M, Kountche BA, Guo X, Zarban RA, Kim D, Al-Babili S, Arold ST. 2018. Structural basis for specific inhibition of the highly sensitive ShHTL7 receptor. *EMBO Reports* **19**: e45619.

- Siodmak A, Hirt H. 2021. New insights into stomatal regulation: role of H(2)S induced persulfidation in ABA signaling. *Molecular Plant* 14: 858–860.
- Suarez-Rodriguez MC, Adams-Phillips L, Liu Y, Wang H, Su SH, Jester PJ, Zhang S, Bent AF, Krysan PJ. 2007. MEKK1 is required for flg22-induced MPK4 activation in Arabidopsis plants. *Plant Physiology* 143: 661–669.
- Suzuki T, Matsushima C, Nishimura S, Higashiyama T, Sasabe M, Machida Y. 2016. Identification of phosphoinositide-binding protein PATELLIN2 as a substrate of Arabidopsis MPK4 MAP kinase during septum formation in cytokinesis. *Plant and Cell Physiology* 57: 1744–1755.
- Takáč T, Vadovič P, Pechan T, Luptovičák I, Šamajová O, Šamaj J. 2016. Comparative proteomic study of Arabidopsis mutants mpk4 and mpk6. *Scientific Reports* 6: 28306.
- Takagi M, Hamano K, Takagi H, Morimoto T, Akimitsu K, Terauchi R, Shirasu K, Ichimura K. 2019. Disruption of the MAMP-induced MEKK1-MKK1/MKK2-MPK4 pathway activates the TNL immune receptor SMN1/RPS6. *Plant and Cell Physiology* 60: 778–787.
- Tanoue T, Adachi M, Moriguchi T, Nishida E. 2000. A conserved docking motif in MAP kinases common to substrates, activators and regulators. *Nature Cell Biology* 2: 110–116.
- Teige M, Scheid E, Eulgem T, Dóczi R, Ichimura K, Shinozaki K, Dangl JL, Hirt H. 2004. The MKK2 pathway mediates cold and salt stress signaling in Arabidopsis. *Molecular Cell* 15: 141–152.
- Völz R, Groß-Hardt R. 2010. Female gametophytic mutants: diagnosis and characterization. In: Hennig L, Köhler C, eds. *Plant developmental biology: methods and protocols*. Totowa, NJ, USA: Humana Press, 143–153.
- Völz R, Harris W, Hirt H, Lee YH. 2022. ROS homeostasis mediated by MPK4 and SUMM2 determines synergid cell death. *Nature Communications* 13: 1746.
- Völz R, Heydlauff J, Ripper D, von Lyncker L, Gross-Hardt R. 2013. Ethylene signaling is required for synergid degeneration and the establishment of a pollen tube block. *Developmental Cell* 25: 310–316.
- Zeng Q, Chen JG, Ellis BE. 2011. AtMPK4 is required for male-specific meiotic cytokinesis in Arabidopsis. *The Plant Journal* 67: 895–906.
- Zhang J, Zhou M, Ge Z, Shen J, Zhou C, Gotor C, Romero LC, Duan X, Liu X, Wu D *et al.* 2020. Abscisic acid-triggered guard cell l-cysteine desulfhydrase function and *in situ* hydrogen sulfide production contributes to heme oxygenase-modulated stomatal closure. *Plant, Cell & Environment* 43: 624–636.
- Zhang J, Zhou M, Zhou H, Zhao D, Gotor C, Romero LC, Shen J, Ge Z, Zhang Z, Shen W *et al.* 2021. Hydrogen sulfide, a signaling molecule in plant stress responses. *Journal of Integrative Plant Biology* 63: 146–160.
- Zhang Z, Liu Y, Huang H, Gao M, Wu D, Kong Q, Zhang Y. 2016. The NLR protein SUMM2 senses the disruption of an immune signaling MAP kinase cascade via CRCK3. *EMBO Reports* 18: 292–302.
- Zhang Z, Wu Y, Gao M, Zhang J, Kong Q, Liu Y, Ba H, Zhou J, Zhang Y. 2012. Disruption of PAMP-induced MAP kinase cascade by a *Pseudomonas syringae* effector activates plant immunity mediated by the NB-LRR protein SUMM2. *Cell Host & Microbe* 11: 253–263.

## Supporting Information

Additional Supporting Information may be found online in the Supporting Information section at the end of the article.

**Fig. S1** MPK4 and its superimposed structure over HsERK2.

**Fig. S2** MPK4 crystal contacts formed by MKK1 dock.

**Fig. S3** Modeling of MPK4 structure in complex with MKK1 and MKK2.

**Fig. S4** Structural model of MPK4 and mutants with docking peptide.

**Fig. S5** Phenotypes of *Arabidopsis thaliana* MPK4 CD motif mutants.

**Fig. S6** Phenotype of *Arabidopsis thaliana* MPK4-C181D mutants.

**Fig. S7** MPK4-C181S and MPK4-C181D localization in *Nicotiana benthamiana* leaf cells.

**Fig. S8** Role of MPK4 CD site on MAPK kinase activity.

**Table S1** List of primers used for genotyping Arabidopsis MPK4 lines.

**Table S2** Primers for cloning and site-directed mutation of Arabidopsis MPK4.

**Table S3** Crystal data collection and refinement statistics of Arabidopsis MPK4.

Please note: Wiley is not responsible for the content or functionality of any Supporting Information supplied by the authors. Any queries (other than missing material) should be directed to the *New Phytologist* Central Office.